Influence of Surface Area Calculation Methods on the Interpretation of LithiumIon Diffusion Coefficient in Graphite Electrodes

ChemElectroChem

Chemistry Europe
European Chemical Societies Publishing
ChemElectroChem

RESEARCH ARTICLE OPEN ACCESS

Influence of Surface Area Calculation Methods on the Interpretation of Lithium-Ion Diffusion Coefficient in Graphite Electrodes

Alessandro Gregucci[1,2] | Antunes Staffolani[1,3] | Francesca Soavi[1,3,4]

[1]Department of Chemistry "Giacomo Ciamician", Alma Mater Studiorum University of Bologna, Bologna, Italy | [2]Department of Applied Science and Technology (DISAT), Politecnico di Torino, Torino Italy | [3]ENERCube lab, Centro Ricerche Energia, Ambiente e Mare, Centro Interdipartimentale per la Ricerca Industriale Fonti Rinnovabili, Ambiente, Mare ed Energia (CIRI-FRAME)—Alma Mater Studiorum University of Bologna, Marina di Ravenna, Ravenna, Italy | [4]National Reference Center for Electrochemical Energy Storage (GISEL)—INSTM, Firenze, Italy

Correspondence: Francesca Soavi (francesca.soavi@unibo.it)

Received: 21 November 2025 | **Revised:** 16 February 2026 | **Accepted:** 25 February 2026

Keywords: batteries | diffusion coefficient | electrochemistry | lithium | mass transport

ABSTRACT

Accurate determination of the lithium-ion diffusion coefficient (D_{Li^+}) is essential for understanding mass-transport limitations in graphite anodes and for improving the performance of lithium-ion batteries. However, the calculation of D_{Li^+} obtained from pulsed electrochemical techniques critically depends on the assumed active surface area, for which no standardized definition currently exists. In this work, we quantitatively assess how different surface area approximations—geometrical area, scanning electron microscopy-derived area, and Brunauer–Emmett–Teller surface area—affect the diffusion coefficient extracted from galvanostatic intermittent titration technique and intermittent current interruption analyses. Both methods were applied to a commercial graphite electrode using an identical dataset, enabling a direct and unbiased comparison of diffusion trends. We show that the choice of surface area leads to variations in D_{Li^+} spanning several orders of magnitude, due to the squared dependence of the area term in the diffusion equation. Overall, our results demonstrate that careful and consistent surface area selection is crucial for reliable diffusion measurements and for ensuring comparability across studies.

1 | Introduction

The growing demand for fast-charging and high power lithium-ion batteries (LIBs) has driven extensive research into their dynamic behaviour [1, 2]. Achieving high-capacity retention during high current operation remains a major challenge for LIBs, as it requires careful consideration of the various processes occurring within their components. The rate capability of a LIB is primarily governed by electrode kinetics—specifically, the rates of electron transfer and lithium-ion transport. Rapid electrode processes minimize over voltages, thereby enhancing the rate performance of the battery. The main component that restricts the high-rate capability of LIBs is the anode, specifically graphite [3, 4], which remains the most commonly used and commercially established anode material. Despite its excellent cycle stability and low operating potential, the formation of the solid electrolyte interphase (SEI) on the graphite surface significantly limits lithium-ion transport across the electrode–electrolyte interface. The SEI introduces additional ionic resistance and slows down Li^+ diffusion kinetics, leading to increased polarization at high charge/discharge rates [5–7]. As a result, commercial LIBs employing graphite anodes are typically constrained to a maximum charge rate of around 1C to prevent excessive overvoltage [1], which can lead to lithium plating on the anode surface and, consequently, loss of performance and safety risks.

Predictive modeling is a powerful approach to speed up the development and the design of LIB electrodes especially for high

power applications. Central to these approaches is the availability of lithium-ion diffusion coefficient (D_{Li^+}) [8] within battery materials, which is critical for guiding the development of new materials [1] and increase the accuracy of modeling of LIBs [9–12]. The diffusion coefficient is a fundamental property in mass transport phenomena that characterizes the mobility of molecules and/or ions in a medium under a concentration gradient [13, 14]. In porous-electrode modeling frameworks, such as those originally proposed by Doyle, Fuller and Newman [15], the solid-state diffusion coefficient directly governs lithium concentration gradients within active material particles and thus determines diffusion-induced polarization under dynamic operating conditions. As a result, inaccuracies in the estimation of the diffusion coefficient can propagate into errors in predicted overpotentials, rate capability, and transport limitations, particularly under fast-charging regimes [3, 9]. In this context, the diffusion coefficient is not merely a fitting parameter, but a physically meaningful quantity that strongly influences the predictive capability of simulations across different length scales. Ensuring a consistent and physically justified determination of the diffusion coefficient is therefore essential for both fundamental understanding and practical battery engineering applications.

When LIBs are charged/discharged, there are changes in the concentration of lithium ions in the bulk of anode active material, electrolyte, and cathode active material and the formation of a concentration gradient along the interphases, including the SEI [15]. Lithium ions have a different mobility inside each of these components [16, 17]; hence, the corresponding lithium-ion diffusion coefficients are different. In a LIB the behaviour of the diffusion is described as nonsteady state diffusion, through the Fick's second law

$$\frac{\partial c_{Li^+}}{\partial t} = D_{Li^+} \frac{\partial^2 c_{Li^+}}{\partial x^2} \tag{1}$$

where c_{Li^+} is the Li-ion concentration while x is the length along which we have the concentration gradient (e.g., particle length) and t is the time.The equation can be solved by applying appropriate boundary conditions [13], which depend on the selected experimental configuration. For example, one common assumption is that at $t = 0$ the Li-ion concentration is uniform throughout the material, while the flux at the surface corresponds to the applied current density.

The commonly used techniques for the solution of the Fick's second law and the determination of D_{Li^+} are galvanostatic intermittent titration technique (GITT) [18], potentiostatic intermittent titration technique [19, 20], intermittent current interruption (ICI) [21], cyclic voltammetry [14], and electrochemical impedance spectroscopy [22].

Among these, the most popular technique is the GITT [23], which is often employed because of its ease of use. The GITT consists of applying a series of constant current (CC) pulses, during which a concentration gradient is generated, followed by rest periods that allow the system to reach a new equilibrium. The D_{Li^+} is then determined by analysing the potential response during the CC step, which reflects the transient behaviour of Li-ion transport inside the active material. Another technique that has recently gained increasing attention is the ICI, which follows a similar experimental approach to the GITT. In this case, however, the estimation of the D_{Li^+} is based on the analysis of the potential relaxation during the rest periods (that are shorter), rather than on the CC steps.

The GITT was first introduced by Weppner and Huggins [18], who also derived the analytical solution of Fick's second law to calculate the diffusion coefficient for a plate-shaped material. However, in LIBs, the active material rarely has a planar geometry. The particles are typically irregular or agglomerated and are often approximated as spherical in diffusion models. For this reason, later studies have demonstrated that the solution proposed by Weppner and Huggins can also be applied to cylindrical and spherical geometries [24]. The full derivation of the diffusion coefficient equation has already been presented in several studies using different approaches [23, 25, 26] and is not reported here. More recently, the ICI technique has gained attention because of its faster and simpler application. As has been demonstrated [21], ICI and GITT techniques share the same analytical solution of Fick's second law. For consistency we will report the equation which has been used by Chien et al. [21]:

$$D_{Li^+} = \frac{4}{\pi}\left(\frac{V}{A}\frac{\frac{\Delta E_{OCV}}{\Delta t_I}}{\frac{dE}{d\sqrt{t}}}\right)^2 \tag{2}$$

where V is the volume of the electrode, A is the surface area, ΔE_{OCV} is the open-circuit voltage (OCV) variation, which is obtained at the end of the rests period for GITT, while for the ICI is obtained as pseudo-OCV through the internal resistance (IR) correction at the last point in which current is applied for each pulse, Δt_I is the total length of the CC period between the rest periods, E is the electrode potential. The parameter t is the time interval in which we have the diffusional process, for the GITT is taken during the current application, while for the ICI is taken from the rest period, as shown in Figure 1.

When GITT and ICI are used to evaluate the D_{Li^+} in the electrodes, they share a common requirement, the knowledge of the active material surface area.These approaches usually assume that this surface area remains constant during the electrochemical process. In practice, many active materials tend to expand and contract during lithiation and delithiation, leading to changes in their real surface area. Hence, it is important to keep in mind that the assumption of a constant surface area might represent a strong approximation. Moreover, the literature shows ambiguity regarding the surface area used in calculating the diffusion coefficient. Ideally, this area should correspond to the electrochemically active surface area [27], which represents the portion of the electrode involved in the electrochemical reactions [28]. However, determining it experimentally is not straightforward, as most electrochemical methods used to estimate it require prior knowledge of the diffusion coefficient.

Therefore, various approximations are commonly adopted. When the active material is available as a powder, the specific surface area of the material is usually considered for the calculation. In cases where only the commercial, composite electrode is available, which includes binder, active material and carbon conductive additive, Hg-porosimetry [10], Brunauer–Emmett–Teller (BET) [29] or scanning electron microscopy (SEM) [12, 30] analyses are adopted. These analyses are performed on the entire electrode to estimate the total surface area, although the BET and Hg-porosimeter measurements also includes contributions from the porosity of inactive components such as binder and

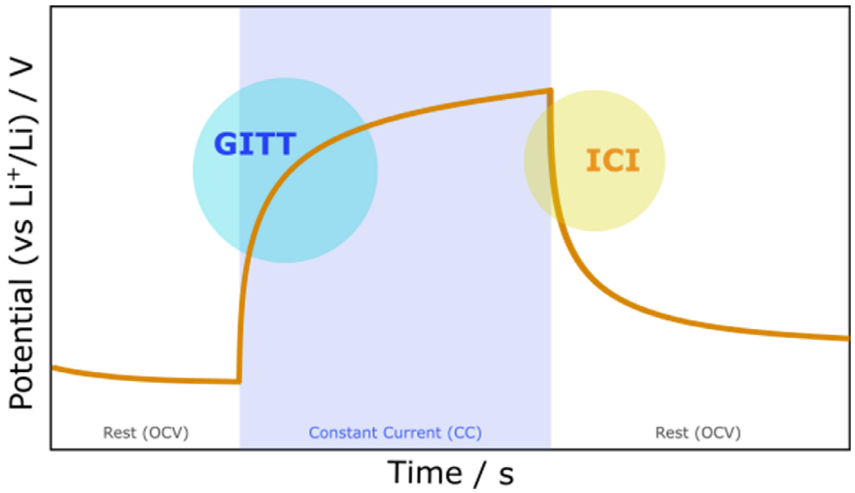

FIGURE 1 | Representative trend of the electrode potential versus time under a GITT pulse. The scheme highlights the instantaneous voltage drop induced by the current step, followed by the gradual relaxation toward equilibrium once the current is interrupted.

conductive additives. In turn, SEM approximation is even stronger and may not reflect the real surface area involved in ion transport. In other cases, researchers simply use the geometrical surface area (GA) of the electrode as an approximation. However, the choice of how to define the surface area can strongly influence the calculated diffusion coefficient. Hence, the purpose of this study is to provide a quantitative assessment of how the assumed surface area affects the determination of the diffusion coefficient. Using both GITT and ICI applied to a commercial graphite anode in a $LiPF_6$- ethylene carbonate (EC): dimethyl carbonate (DMC) 1:1 electrolyte, we show that the value of the calculated diffusion coefficient can vary by several orders of magnitude depending on the surface area approximation, underlining the need for a consistent approach in diffusion studies of lithium-ion battery electrodes.

2 | Experimental Section

2.1 | Electrochemical Cell Assembly and Test

A commercial graphite electrode (NANOMYTE BE-200E, NEI), containing 90% of graphite, 5% of polyvinylidene fluoride (PVDF) binder and 5% of carbon black, with a graphite mass loading of 6.6 mg cm^{-2} was selected for this study. Before cell assembly, the electrodes were cut into 9 mm disks and dried overnight under vacuum at 120°C using a Büchi B-585 oven. The experiments were carried out in T-shaped three electrodes Teflon cells (BOLA, Bohlender GmbH), each containing 200 µL of an electrolyte composed of 1 M $LiPF_6$ in a 1:1 (v:v) mixture of EC and DMC (LP30, Solvionic). Commercial Whatman GF/D glass fiber disk (10 mm diameter) was used as separator, after being dried under vacuum at 120°C in a glass oven overnight (Büchi B-585). The cells operated in a three-electrode half-cell configuration, with two lithium metal disks (10 mm diameter) serving as counter and quasi-reference electrodes. All assembly steps were performed in an argon-filled glovebox (MBraun) with oxygen and water levels below 0.1 ppm. Cell testing was conducted at 30°C. The formation process consisted of one cycle at C/20 (18.6 mA g^{-1}) with a CC–CV–CC protocol (constant current–constant voltage–costant current) between 1.5 and 0.02 V versus Li^+/Li. The CV step was performed at 0.02 V versus Li^+/Li with a current cut-off of C/80 (4.64 mA g^{-1}) or a maximum duration of 1 h, then the cell has been cycled four times at C/5 (74.3 mA g^{-1}) under the same protocol, using a VMP-3 galvanostat/potentiostat/frequency analyzer (Biologic). After cycling, the GITT was applied. Each GITT step (even called titration step) consisted of a 15 min constant-current pulse at C/10 (37.1 mA g^{-1}) followed by a 45 min relaxation at OCV. The titration steps were repeated until reaching the (de-)lithiation cut-off potentials. The electrode potential range was maintained between 1 and 0.02 V versus Li^+/Li. All the potential values here reported refers to the redox couple Li^+/Li. The ICI analysis was performed using exactly the same data collected during the GITT experiment, without any additional cycling. The main difference between the two methods lies in how the diffusion coefficient is extracted: GITT analyses the voltage response during the current pulse and obtain the OCV curve from the relaxation period, while ICI determines the diffusion coefficient from the early-stage voltage relaxation that follow brief current interruptions, and uses a pseudo-OCV obtained by removing the IR drop from the last point in which the current is applied. As a result, both techniques rely on the same dataset but apply different analytical approaches to estimate the Li^+ diffusion coefficient. $dE/d\sqrt{t}$ is obtained from the slope of the plot of the electrode potential versus the square root of the time. The time interval used for the fit was 25–225 s for GITT and 1–50 s for ICI. For GITT, time zero corresponds to the start of the current pulse, while for ICI it corresponds to the beginning of the relaxation period.

Data analysis was performed using a custom Python script.

2.2 | Surface Area Evaluation

The geometrical approximated (GA) surface area, is easily obtained as the surface of the electrode disk used for the test; in this work, the electrode disk diameter was of 9 mm, so the GA area is of 6.36×10^{-5} m^2. The surface area reported by the manufacturer in the electrode datasheet for the active material, obtained with BET, was of 6.33×10^{-3} m^2. Additionally, we have evaluated the SEM approximated surface area [30]. The approximation consists on estimating the mean particle radius, in this

work has been obtained from SEM (Crossbeam 350, Zeiss) image with the open-source software imageJ [31] by measuring the particle size along two orthogonal direction for each particle, then each particle has been approximated to be spherical and so it was possible to calculate the particle volume (V_p) and the surface area of the particle (S_p) with the following equations

$$V_p = \frac{4}{3}\pi R_p^3 \tag{3}$$

$$S_p = 4\pi R_p^2 \tag{4}$$

The total active material volume (V_{AM}) can be obtained by multiplying the electrode volume (V_{el}) and the active material fraction (ε_{AM}). The electrode volume is obtained from the surface area of the electrode (S_{el}) and the thickness of the electrode (L). It is important to note that V_{AM} is an approximation. This approach assumes that the corresponding fraction of the electrode volume is fully occupied by active material, and it does not account for the porosity of the electrode or the individual densities of each component of the formulation.

$$V_{AM} = \varepsilon_{AM} V_{el} = \varepsilon_{AM} S_{el} L \tag{5}$$

The amount of active material particles (N_{AM}) that can fit in the electrode can be then be calculated by knowing V_{AM} and V_p, as here reported

$$N_{AM} = \frac{V_{AM}}{V_p} \tag{6}$$

The total surface area of the active material (S_{AM}) can be obtained by multiplying N_{AM} and the S_p

$$S_{AM} = N_{AM} S_p \tag{7}$$

3 | Results and Discussion

Figure 2 reports the SEM image of the graphite electrode that was used to determine the particle size and electrode surface as described in Section 2.2. The mean particle diameter resulted to be 18 μm ($R_p = 9\mu m$) and the thickness of the electrode was $L = 64\mu m$ (without the Cu current collector) for a total surface area (A_{SEM}) of 1.29×10^{-3} m^2. The A_{SEM} is reported in Table 1 along with the values of electrode surface evaluated by different methods, namely the geometrial area (A_{GA}) and the BET surface area (A_{BET}). The GA provides the lowest surface area value, being A_{GA} equal to 6.36×10^{-5} m^2, since it considers only the external geometry (foot print) of the electrode. In contrast, the BET method yields the highest value of surface A_{BET} equal to 6.33×10^{-3} m^2, as it captures the micro- and mesoporosity of the active material that are not visible in SEM images or considered in simple geometric estimations. Table 1 highlights that the surface area estimated from SEM image analysis, A_{SEM} lies between the two extremes, i.e., A_{GA} and A_{BET}, as it approximately accounts for particle morphology.

3.1 | Calculation of the Diffusion Coefficient

Figure 3 shows the trend of the graphite electrode potential over time during the GITT experiment for both lithiation and

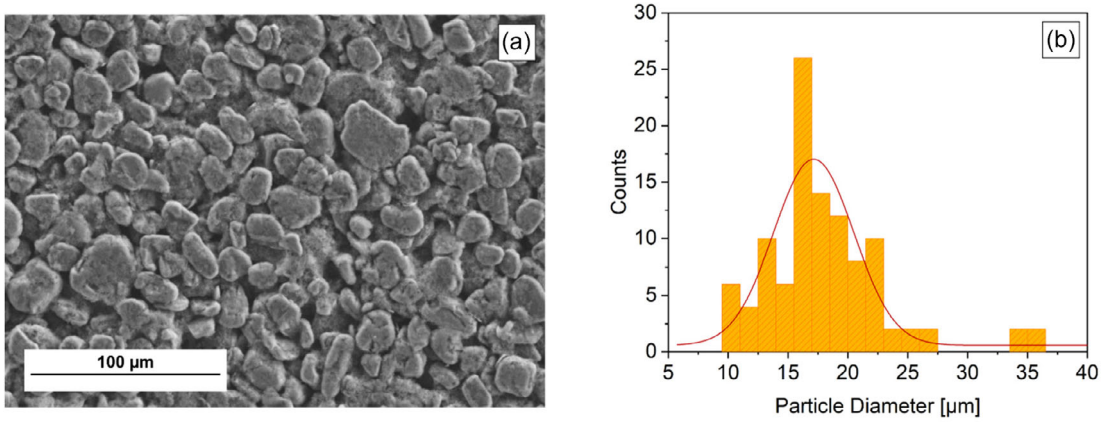

FIGURE 2 | (a) SEM image acquired at 5 kV and ×1000 magnification and (b) distribution of particle sizes of the commercial graphite electrode.

TABLE 1 | Reports the surface areas determined by the GA (A_{GA}), by SEM (A_{SEM}), and BET (A_{BET}) measurements, along with the mean diffusion coefficients obtained using each area during both lithiation and delithiation by GITT ($D_{Li^+}^{GITT}$) and ICI ($D_{Li^+}^{ICI}$).

		Lithiation[a]				Delithiation			
	Area, m^2	DA^2, cm^6 s^{-1}	$D_{Li^+}^{GITT}$, cm^2 s^{-1}	DA^2, cm^6 s^{-1}	$D_{Li^+}^{ICI}$, cm^2 s^{-1}	DA^2, cm^6 s^{-1}	$D_{Li^+}^{GITT}$, cm^2 s^{-1}	DA^2, cm^6 s^{-1}	$D_{Li^+}^{ICI}$, cm^2 s^{-1}
A_{GA}	6.36×10^{-5}	8.3×10^{-10}	2.1×10^{-9}	5.9×10^{-9}	1.5×10^{-8}	2.0×10^{-9}	5.1×10^{-9}	1.3×10^{-8}	3.2×10^{-8}
A_{SEM}	1.29×10^{-3}		5.0×10^{-12}		3.5×10^{-11}		1.2×10^{-11}		7.8×10^{-11}
A_{BET}	6.33×10^{-3}		2.1×10^{-13}		1.5×10^{-12}		5.2×10^{-13}		3.2×10^{-12}

[a]The table also includes the surface-area-independent diffusion coefficient (DA^2), which enables the evaluation of how each surface area definition influences the calculated D_{Li^+} values for the graphite electrode.

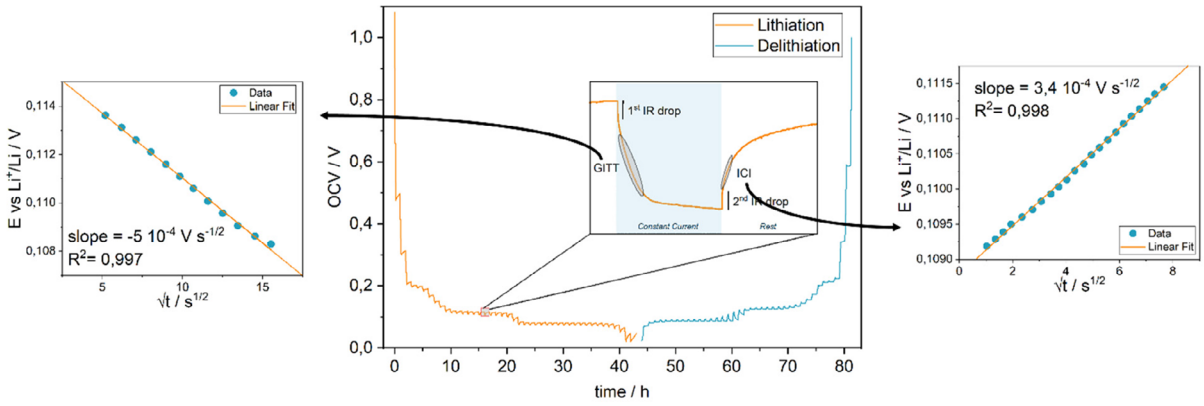

FIGURE 3 | GITT and ICI profiles of a graphite electrode tested in a three-electrode cell. The left and right insets show the linear fit of $dE/d\sqrt{t}$, for both the approaches.

delithiation. The electrode potential profile clearly displays the sequence of current pulses and relaxation periods that characterise the GITT protocol. During each step, the constant-current pulse produces a rapid potential change followed by a relaxation at open circuit. This step provides the data needed to evaluate the diffusion-controlled voltage evolution. Indeed, the electrode potential is plotted versus the square root of the time to get the linear trend and the corresponding slope $dE/d\sqrt{t}$, needed to solve Equation (2) . Figure 3 reports examples of the linear E versus $\sqrt{t}$ plots, the corresponding fitted lines and the calculated slopes $dE/\sqrt{t}$ for both GITT and ICI. The time interval of 25–225 s for GITT and 1–50 s for ICI was selected so that the linear fits of all pulses exhibited an R^2 value higher than 0.99. For GITT, the slope is obtained from the initial transient after each current pulse. For the ICI method, the diffusion analysis is applied to the same data by using the potential relaxation. Because both methods are applied to the same measurements, the comparison between GITT and ICI is not influenced by differences in experimental conditions. Showing the fitting procedure for the two techniques on the same dataset highlights how GITT and ICI extract diffusion information from different segments of the voltage response. This provides a consistent basis for the comparison of the diffusion coefficients presented in the next figures.

Figure 4 reports the values of the graphite electrode potentials in open circuit conditions (OCV) during lithiation (Figure 4a) and delithation (Figure 4b), as a solid line. From the OCV profile we can observe that the graphite shows three plateaux, the first is observed around 5–15% SOC, is generally associated with the $LiC_{24} \rightarrow LiC_{18}$ transition. The second plateau, between 25 and 50% SOC, corresponds to $LiC_{18} \rightarrow LiC_{12}$ and the third, from 55% to 95% SOC, to $LiC_{12} \rightarrow LiC_6$ [32].

Figure 4 also reports the trends of the surface-area-independent diffusion coefficients (DA^2) obtained from GITT and ICI in the voltage range $0.02\,V < U < 1.5\,V$ versus Li^+/Li. In this work, DA^2 is used as a quantity that allows us to remove the explicit contribution of the surface area from the diffusion equation. Because the choice of the surface area approximation can strongly influence the final value of D_{Li^+}, analysing DA^2 makes it possible to compare the results from GITT and ICI without introducing any surface-area-related bias. Following the Equation (2), DA^2 is described by

$$DA^2 = \frac{4}{\pi}\left(V\frac{\frac{\Delta E_{OCV}}{\Delta t_I}}{\frac{dE}{d\sqrt{t}}}\right)^2 \tag{8}$$

Both techniques provide DA^2 trends that show a clear minimum in correspondence of the different OCV plateau.This behaviour can be assessed to two possible reasons. First, in these regions the graphite de(lithiation) does not occur via a solid solution mechanism. Rather, the (de)lithiation proceeds via a two-phases

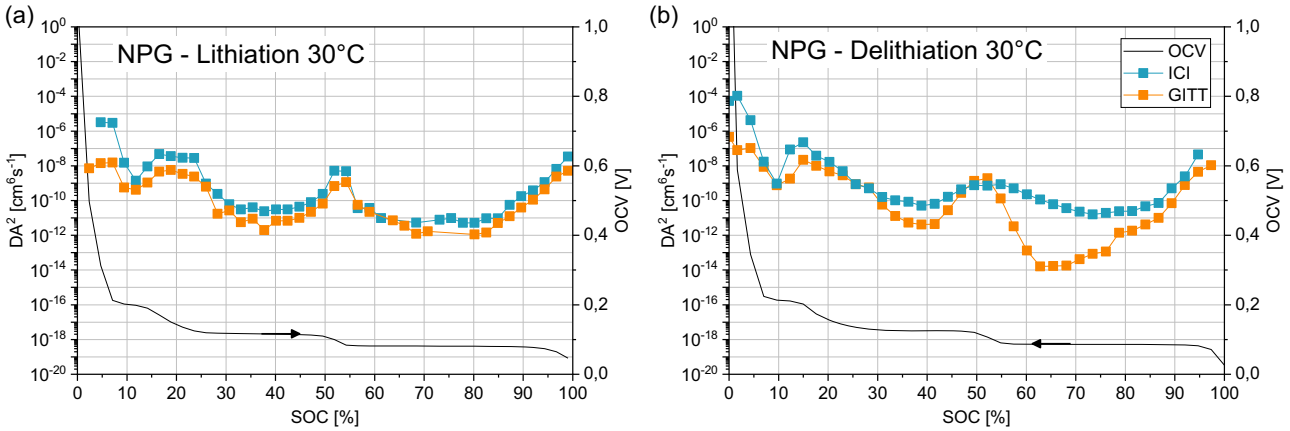

FIGURE 4 | Trends of the electrode potential in open circuit condition (OCV, solid line) and of the surface area independent diffusion coefficients (DA^2) obtained from ICI and GITT during (a) lithiation and (b) delithiation of the graphite electrode.

equilibrium between two Li_xC_6 phases with different Li concentrations. The SoC changes predominantly through variation of the Li_xC_6 phase fractions, while the lithium chemical potentials of the coexisting phases remain nearly constant. As a consequence, during the plateau regions the term $dE/d\sqrt{t}$ approaches zero. Since the conventional GITT (and ICI) expression (Equation (2)) contains the term $(dE/d\sqrt{t})^2$, the calculated diffusion coefficient artificially shows local minimum in correspondence of the plateau regions and can even approach values close to zero. Second, in a two-phase equilibrium, the rate-limiting mechanism is not purely the Fickian diffusion, but rather the moving phase boundary within each phase coupled to interfacial transformation kinetics (a Stefan problem for moving boundaries between two phases) [32]. Thus, the diffusion coefficient measurement is affected by a large underestimation error.

During lithiation, the diffusion coefficients obtained from GITT and ICI show good agreement. A similar trend is found during delithiation, although in the range 55%–95% SOC some deviations appear. In this range, a sharp decrease of DA^2_{GITT} can be observed that is not present in the case of the ICI technique. This discrepancy can be related to two reasons. On one side, it should be considered that DA^2 calculation requires the analysis of the electrode potential that in GITT, unlike in ICI, is affected by electrode kinetics under current flow. When a current pulse is applied, several processes occur sequentially: an initial ohmic loss (IR drop), followed by charge–transfer at short times, and finally solid-state diffusion, which dominates at longer times [33]. In practice, these processes may partially overlap, especially during the first seconds of the measurement. As a consequence, the identification of a purely diffusion-controlled regime in GITT can be challenging, leading to uncertainty in the estimation of the diffusion coefficients [34]. In ICI instead after IR drop, the only process that remains active is the diffusion process [21], making it easier to estimate the diffusion coefficient. Therefore, the values derived from ICI are likely to be more accurate for assessing the Li-ion diffusion behaviour in that region. Another possible reason for those deviations of DA^2_{GITT} from DA^2_{ICI} in Figure 4 is related to a pure mathematical issue. Indeed, the solution of GITT equation requires that electrode potential changes in relation to the applied current. Hence, it hardly can be applied in the 55%–95% SOC region, where OCV is not changing. The nearly constant equilibrium potential makes the term linking the potential variation to the change in lithium concentration so low to lead to large uncertainties in the extracted diffusion coefficients [35]. By contrast, the use of a pseudo-OCV introduces an effective slope of the equilibrium potential in a narrow SOC range, allowing the ICI formalism to remain numerically stable and thus reducing the associated error.

Figure 5 shows the effect of using different surface area approximations on the diffusion coefficient calculated from the ICI method. Three approaches were considered: the GA, the estimation from SEM image analysis, and the surface area measured by BET reported in Table 1. As discussed above, each method represents a different level of accuracy in describing the electrode surface and its active sites. The results indicate a clear trend: the use of A_{GA} produces the highest diffusion coefficient values, followed by the SEM approximation (A_{SEM}), while the values obtained by using A_{BET} are the lowest. This behaviour is consistent with Equation (2), where the surface area appears in the denominator. Therefore, a higher surface area leads to a smaller diffusion coefficient. The effect becomes even more pronounced because the area term is squared in the equation, meaning that small differences in surface area can generate large variations in the calculated diffusion coefficient.

As reported in Table 1, the diffusion coefficient average over the full lithiation/delithiation process can vary by several orders of magnitude depending on the chosen approximation. This difference is not only a mathematical consequence of the equation but also reflects the physical complexity of the electrode surface, where roughness and porosity significantly influence the real electrochemical active area. These results show that the estimation of the surface area has a strong impact on the diffusion coefficient calculation.

The A_{SEM} approximates the active material particles as ideal solid spheres with identical dimensions. This simplification neglects intrinsic particle features such as shape irregularities and internal porosity [27], which contribute to the true active surface area. As a consequence, the SEM-derived surface area (A_{SEM}) may underestimate the effective active area and thus bias the diffusion coefficient toward higher values. In addition, SEM analysis typically considers only particles located at the electrode surface and implicitly assumes a uniform distribution of the active material throughout the electrode thickness, an assumption that is not always valid, particularly for laboratory-scale electrodes. Conversely, the A_{BET} evaluated on the whole electrode is affected

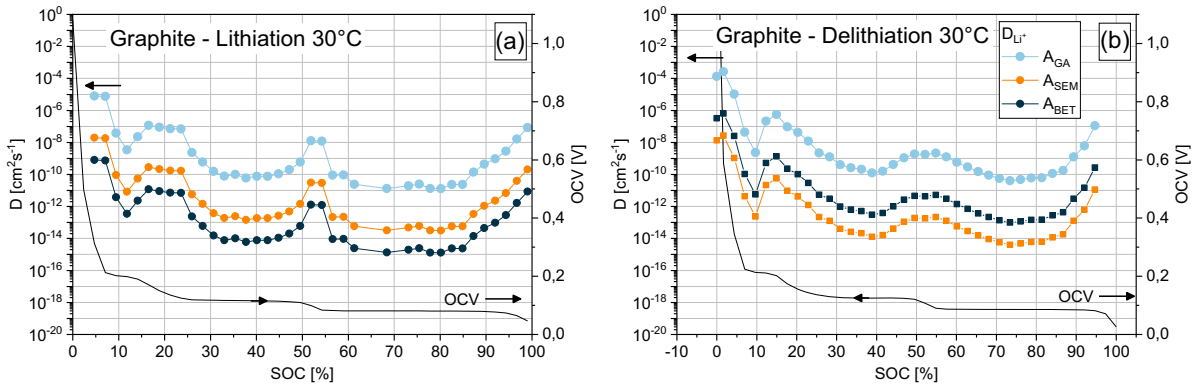

FIGURE 5 | Trends of the electrode potential in open circuit condition (OCV, solid line) and of the lithium-ion diffusion coefficients obtained from ICI using different values of electrode area, during (a) lithiation and (b) delithiation of the graphite electrode.

by the contribution of all components, such as binder, conductive additives, and active material. The polymeric binder might occlude the active material microporosity and impede the full access of ions to the active material bulk [36, 37]. In turn, the carbon conductive additive might contribute to the composite specific area. If A_{BET} is evaluated on the pure active material, it generally leads to an overestimation of the surface area exposed to the electrolyte and, consequently, to lower derived diffusion coefficients. In this context, the electrode formulation becomes a relevant parameter, as variations in the proportion of active material can significantly affect the measured BET surface area. When the active material content is relatively low, the influence of nonactive components becomes more pronounced, which must be considered when the objective is to characterize bulk transport properties.

Among the methods considered in this work, the real electrochemical surface area is therefore expected to fall between the SEM- and BET-based estimates, as supported by comparisons with literature data obtained using nonelectrochemical techniques, such as time-domain nuclear magnetic resonance [38, 39]. In electrochemical modeling, diffusion coefficients strongly influence predicted transport limitations [11]. Within porous-electrode frameworks, the solid-state diffusion coefficient governs the development of lithium concentration gradients inside active material particles and therefore directly affects diffusion-induced overpotentials during dynamic operation. Overestimated diffusion coefficients may artificially suppress diffusion-controlled polarization, leading to unrealistically optimistic predictions of rate capability. Conversely, underestimated diffusion coefficients may exaggerate solid-state transport resistance, overpredict lithium concentration heterogeneities within the electrode, which are known to impact on the estimated electrode cyclability. Since diffusion parameters are often used for model parameterization and validation [10, 12], systematic errors in the estimation of the diffusion coefficient can propagate into misinterpretation of kinetic limitations, and incorrect identification of the dominant rate-limiting mechanism [9]. These inaccuracies become particularly critical under fast-charging conditions, where steep concentration gradients develop and diffusion limitations compete with interfacial kinetics and ohmic drops. In such regimes, even moderate deviations in the diffusion coefficient may significantly alter the predicted lithium distribution, local overpotentials, and, consequently, the estimated risk of lithium plating [40, 41]. Therefore, uncertainties in the experimental determination of diffusion coefficient are not confined to material characterization but may compromise the predictive reliability of electrochemical simulations across multiple operating conditions. For this reason, effective diffusion coefficients that account for electrode microstructure such as BET and SEM rather than geometrical surface area approximations should be encouraged as reported in other works [10, 12]. The A_{GA} should be adopted only when alternative approaches are not available and, even in this case, it should be regarded as a strong estimation of the diffusion coefficient. The associated error can be reduced only by minimizing electrode thickness, thereby limiting deviations from the assumptions underlying the geometric model. As a rule of thumb, we consider as thin those electrodes featuring graphite mass loading lower than 1 mg/cm^2, while thick electrodes exhibit loadings above 10 mg/cm^2.

4 | Conclusion

This study shows that, in the case of a commercial graphite electrode, the lithium-ion diffusion coefficients obtained from the ICI method are in strong agreement with those derived from GITT, confirming the reliability of both techniques. The ICI method can also be easily integrated in the data analysis of pulsed techniques as a complementary tool to verify the correct calibration of the experimental setup and to provide additional control during diffusion studies. The analysis demonstrated that the choice of surface area approximation has a significant impact on the calculated D_{Li^+} values. Since the surface area appears squared in the diffusion equation, even small variations in its estimation can produce large differences in the results. As shown in Table 1, for the investigated commercial porous graphite electrode (mass loading of 6.6 mg cm^{-2}), the use of geometrical, SEM-derived, or BET surface areas leads to diffusion coefficients differing by several orders of magnitude. In particular, the geometric surface area (A_{GA}) does not adequately represent the electrochemically active surface of a composite porous electrode and results in a significant overestimation of the diffusion coefficient. In such cases, surface characterization based on BET or SEM analysis is recommended to obtain more reliable and comparable diffusion data. Overall, these findings highlight the importance of a consistent and accurate surface area determination when evaluating lithium-ion diffusion in battery materials.

Author Contributions

Alessandro Gregucci: conceptualization (lead); data curation (lead); formal analysis (lead); investigation (lead); methodology (lead); writing – original draft (lead). **Antunes Staffolani**: investigation (supporting); methodology (supporting); writing – review & editing (supporting). **Francesca Soavi**: conceptualization (equal); project administration (lead); resources (lead); supervision (lead); writing – review & editing (lead).

Acknowledgments

Francesca Soavi and Antunes Staffolani acknowledge MOST—Sustainable Mobility Center project, funded by the European Union Next-Generation EU (PIANO NAZIONALE DI RIPRESA E RESILIENZA (PNRR) e MISSIONE 4 COMPONENTE 2, INVESTIMENTO 1.4 e D.D. 1033 17/06/2022, CN00000023). This manuscript reflects only the authors' views and opinions; neither the European Union nor the European Commission can be considered responsible for them.

Open access publishing facilitated by Universita degli Studi di Bologna, as part of the Wiley - CRUI-CARE agreement.

Funding

This work was supported by the European Union Next-Generation (EU) (CN00000023).

Conflicts of Interest

The authors declare no conflicts of interest.

Data Availability Statement

Data for this article are available at https://amsacta.unibo.it/id/eprint/8858.

References

1. M. Weiss, R. Ruess, J. Kasnatscheew, et al., "Fast Charging of Lithium-Ion Batteries: A Review of Materials Aspects," *Advanced Energy Materials* 1 (2021): 2002891, https://doi.org/10.1002/aenm.202101126.

2. A. Tomaszewska, Z. Chu, X. Feng, et al., "Lithium-Ion Battery Fast Charging: A Review," *eTransportation* 1 (2019): 100011, https://doi.org/10.1016/j.etran.2019.100011.

3. S. Weng, G. Yang, S. Zhang, et al., "Kinetic Limits of Graphite Anode for Fast-Charging Lithium-Ion Batteries," *Nano-Micro Letters* 15 (2023): 215, https://doi.org/10.1007/s40820-023-01183-6.

4. Y.-X. Yao, L. Xu, C. Yan, and Q. Zhang, "Principles and Trends in Extreme Fast Charging Lithium-Ion Batteries," *EES Batteries* 1 (2025): 4–22, https://doi.org/10.1039/D4EB00011K.

5. A. Wang, S. Kadam, H. Li, S. Shi, and Y. Qi, "Review on Modeling of the Anode Solid Electrolyte Interphase (SEI) for Lithium-Ion Batteries," *Npj Computational Materials* 4 (2018): 15, https://doi.org/10.1038/s41524-018-0064-0.

6. H. Adenusi, G. A. Chass, S. Passerini, K. V. Tian, and G. Chen, "Lithium Batteries and the Solid Electrolyte Interphase (SEI)—Progress and Outlook," *Advanced Energy Materials* 13 (2023): 2203307, https://doi.org/10.1002/aenm.202203307.

7. L. von Kolzenberg, A. Latz, B. Horstmann, "Solid-Electrolyte Interphase During Battery Cycling: Theory of Growth Regimes," *ChemSusChem* 13 (2020): 3901–3910, https://doi.org/10.1002/cssc.202000867.

8. T. Schied, A. Nickol, C. Heubner, et al., "Determining the Diffusion Coefficient of Lithium Insertion Cathodes from GITT Measurements: Theoretical Analysis for Low Temperatures," *ChemPhysChem* 22 (2021): 885–890.https://doi.org/10.1002/cphc.202001025.

9. H. Lee, S. Yang, S. Kim, et al., "Understanding the Effects of Diffusion Coefficient and Exchange Current Density on the Electrochemical Model of Lithium-Ion Batteries," *Current Opinion in Electrochemistry* 34 (2022): 100986, https://doi.org/10.1016/j.coelec.2022.100986.

10. M. Ecker, T. K. D. Tran, P. Dechent, S. Käbitz, A. Warnecke, and D. U. Sauer, "Parameterization of a Physico-Chemical Model of a Lithium-Ion Battery: I. Determination of Parameters," *Journal of The Electrochemical Society* 162 (2015): A1836–A1840.https://doi.org/10.1149/2.0551509jes.

11. M. Ecker, S. Käbitz, I. Laresgoiti, and D. U. Sauer, "Parameterization of a Physico-Chemical Model of a Lithium-Ion Battery: II. Model Validation," *Journal of The Electrochemical Society* 162 (2015): A1849–A1857.https://doi.org/10.1149/2.0541509jes.

12. C.-H. Chen, F. Brosa Planella, K. O'Regan, D. Gastol, W. D. Widanage, and E. Kendrick, "Development of Experimental Techniques for Parameterization of Multi-Scale Lithium-Ion Battery Models," *Journal of the Electrochemical Society* 167 (2020): 080534, https://doi.org/10.1149/1945-7111/ab9050.

13. J. Crank, *The Mathematics of Diffusion* (Oxford University Press, 1975).

14. A. J. Bard, L. R. Faulkner and H. S. White, *Electrochemical Methods: Fundamentals and Applications* (2022).

15. M. Doyle, T. F. Fuller, and J. Newman, "Modeling of Galvanostatic Charge and Discharge of the Lithium/Polymer/Insertion Cell," *Journal of the Electrochemical Society* 140 (1993): 1526–1533,https://doi.org/10.1149/1.2221597

16. J. B. Goodenough and K.-S. Park, "The Li-Ion Rechargeable Battery: A Perspective," *Journal of the American Chemical Society* 135 (2013): 1167–1176, https://doi.org/10.1021/ja3091438.

17. G. Li, "Regulating Mass Transport Behavior for High-Performance Lithium Metal Batteries and Fast-Charging Lithium-Ion Batteries," *Advanced Energy Materials* 11 (2021): 2002891, https://doi.org/10.1002/aenm.202002891.

18. W. Weppner and R. A. Huggins, "Determination of the Kinetic Parameters of Mixed-Conducting Electrodes and Application to the System Li3Sb," *Journal of the Electrochemical Society* 124 (1977): 1569–1578, https://doi.org/10.1149/1.2133112.

19. C. J. Wen, B. A. Boukamp, R. A. Huggins, and W. Weppner, "Thermodynamic and Mass Transport Properties of " LiAl ," *Journal of the Electrochemical Society* 126 (1979): 1979–2266, https://doi.org/10.1149/1.2128939.

20. W. Weppner and R. A. Huggins, "Electrochemical Methods for Determining Kinetic Properties of Solids," *Annual Review of Materials Science* 8 (1978): 269–311, https://doi.org/10.1146/annurev.ms.08.080178.001413.

21. Y.-C. Chien, H. Liu, A. S. Menon, W. R. Brant, D. Brandell, and M. J. Lacey, "Rapid Determination of Solid-State Diffusion Coefficients in Li-Based Batteries via Intermittent Current Interruption Method," *Nature Communications* 14 (2023): 2289, https://doi.org/10.1038/s41467-023-37989-6.

22. C. Ho, I. D. Raistrick, and R. A. Huggins, "Application of A-C Techniques to the Study of Lithium Diffusion in Tungsten Trioxide Thin Films," *Journal of the Electrochemical Society* 127 (1980): 343–350, https://doi.org/10.1149/1.2129668.

23. M. Jia, W. Zhang, X. Cai, et al., "Re-Understanding the Galvanostatic Intermittent Titration Technique: Pitfalls in Evaluation of Diffusion Coefficients and Rational Suggestions," *Journal of Power Sources* 543 (2022): 231843, https://doi.org/10.1016/j.jpowsour.2022.231843.

24. C. Deng and W. Lu, "Consistent Diffusivity Measurement between Galvanostatic Intermittent Titration Technique and Electrochemical Impedance Spectroscopy," *Journal of Power Sources* 473 (2020): 228613, https://doi.org/10.1016/j.jpowsour.2020.228613.

25. A. Nickol, T. Schied, C. Heubner, et al., "GITT Analysis of Lithium Insertion Cathodes for Determining the Lithium Diffusion Coefficient at Low Temperature: Challenges and Pitfalls," *Journal of the Electrochemical Society* 167 (2020): 090546, https://doi.org/10.1149/1945-7111/ab9404.

26. J. Kim, S. Park, S. Hwang, and W.-S. Yoon, "Principles and Applications of Galvanostatic Intermittent Titration Technique for Lithium-Ion Batteries," *Journal of Electrochemical Science and Technology* 13 (2022): 19–31, https://doi.org/10.33961/jecst.2021.00836.

27. L. Pfaffmann, C. Birkenmaier, M. Müller, et al., "Investigation of the Electrochemically Active Surface Area and Lithium Diffusion in Graphite Anodes by a Novel OsO4 Staining Method," *Journal of Power Sources* 307 (2016): 762–771, https://doi.org/10.1016/j.jpowsour.2015.12.085.

28. K. Ariyoshi and T. Tanaka, "Effect of Electrochemically Active Surface Area on the Charge-Transfer Resistance of Layered Positive Electrode Materials," *CrystEngComm* 27, no. 37 (2025): 6122–6126, https://doi.org/10.1039/D5CE00709G.

29. T. Beuse, M. Fingerle, C. Wagner, M. Winter, and M. Börner, "Comprehensive Insights into the Porosity of Lithium-Ion Battery Electrodes: A Comparative Study on Positive Electrodes Based on LiNi0.6Mn0.2Co0.2O2 (NMC622)," *Batteries* 7 (2021): 70, https://doi.org/10.3390/batteries7040070.

30. A. Verma, K. Smith, S. Santhanagopalan, D. Abraham, K. P. Yao, and P. P. Mukherjee, "Galvanostatic Intermittent Titration and Performance Based Analysis of $LiNi_{0.5}Co_{0.2}Mn_{0.3}O_2$ Cathode," *Journal of the Electrochemical Society* 164, no. 13 (2017): A3380–A3392, https://doi.org/10.1149/2.1701713jes.

31. C. A. Schneider, W. S. Rasband, and K. W. Eliceiri, "NIH Image to ImageJ: 25 Years of Image Analysis," *Nature Methods* 9, no. 7 (2012): 671–675, https://doi.org/10.1038/nmeth.2089.

32. S. Koga and M. Krstic, "State Estimation of the Stefan PDE: A Tutorial on Design and Applications to Polar Ice and Batteries," *Annual Reviews in Control* 53 (2022): 199–223, https://doi.org/10.1016/j.arcontrol.2022.02.001.

33. A. Barai, K. Uddin, W. D. Widanage, A. McGordon, and P. Jennings, "A Study of the Influence of Measurement Timescale on Internal Resistance Characterisation Methodologies for Lithium-Ion Cells," *Scientific Reports* 8 (2018): 21, https://doi.org/10.1038/s41598-017-18424-5.

34. E. Deiss, Spurious Chemical Diffusion Coefficients of Li+ in Electrode Materials Evaluated with GITT, *Electrochimica Acta* 50, 14 (2005): 2927–2932, https://doi.org/10.1016/j.electacta.2004.11.042.

35. C. Delacourt, M. Ati, and J. M. Tarascon, "Measurement of Lithium Diffusion Coefficient in Li_y $FeSO_4$ F," *Journal of the Electrochemical Society* 158 (2011): A741–A749, https://doi.org/10.1149/1.3581087.

36. A. Missiroli, F. Soavi, and M. Mastragostino, "Increased Performance of Electrodeposited PtRu/C-Nafion Catalysts for DMFC," *Electrochemical and Solid-State Letters* 8, no. 2 (2005): A110, https://doi.org/10.1149/1.1847686.

37. M. Mastragostino, A. Missiroli, and F. Soavi, "Carbon Supports for Electrodeposited Pt-Ru Catalysts for DMFCs," *Journal of the Electrochemical Society* 151, no. 11 (2004): A1919, https://doi.org/10.1149/1.1805751.

38. J. Langer, V. Epp, P. Heitjans, F. A. Mautner, and M. Wilkening, "Lithium Motion in the Anode Material LiC. 6 as Seen via Time-Domain 7 Li NMR," *Physical Review B* 88 (2013): 094304, https://doi.org/10.1103/PhysRevB.88.094304.

39. K. Toyoura, Y. Koyama, A. Kuwabara, F. Oba, and I. Tanaka, "First-Principles Approach to Chemical Diffusion of Lithium Atoms in a Graphite Intercalation Compound," *Physical Review B* 78 (2008): 214303, https://doi.org/10.1103/PhysRevB.78.214303.

40. K. Smith and C.-Y. Wang, "Power and Thermal Characterization of a Lithium-Ion Battery Pack for Hybrid-Electric Vehicles," *Journal of Power Sources* 160, no. 7 (2006): 662–673, https://doi.org/10.1016/j.jpowsour.2006.01.038.

41. X.-G. Yang, Y. Leng, G. Zhang, S. Ge, and C.-Y. Wang, "Modeling of Lithium Plating Induced Aging of Lithium-Ion Batteries: Transition from Linear to Nonlinear Aging," *Journal of Power Sources* 360 (2017): 28–40, https://doi.org/10.1016/j.jpowsour.2017.05.110.